Geochemical and tectonic characteristics of manganese mineralization in the Yozgat region, Turkey

Nursel ÖKSÜZ[1], İsmail KOÇAK[2, *] and Uğur TEMIZ[1]

[1] Bozok University, Department of Geological Engineering, Yozgat, Turkey

[2] Bandırma Onyedi Eylül University, Department of Engineering Science, Faculty of Engineering and Natural Sciences, Balıkesir, Turkey

North of the Central Anatolian Crystalline Complex and bordered by the İzmir–Ankara–Erzincan Suture Zone, mineralization occurs within ophiolites known as Anatolian Ophiolite Complex. The mineralization is present within banded, laminated and lenticular radiolarites which are intensely fractured and folded. It is distributed around Derbent, Baltasarilar, Cihanpasa, Buyukmahal, Eymir and Kadisehri where pyrolusite, psilomelane, manganite and braunite comprise the main paragenesis and jacobsite, magnetite, limonite and goethite are minor phases. The negative Eu anomaly suggests that the hydrothermal source was distant from the mineralization area or was mixed with seawater. All samples from the Cihanpasa and Buyukmahal areas have a negative Ce anomaly and resemble low-temperature hydrothermal mineral deposits. Samples from other locations (Derbent, Baltasarilar, Cihanpasa, Eymir, Buyukmahal, Tarhana) are characterized by both negative and positive Ce anomalies. From this it can be inferred that both hydrothermal and hydrogenetic processes were active in mineralization. High Ba contents and a LREE-enriched pattern together with negative Ce anomalies and trace element distributions indicate that the mineralization in the area was derived from a primary hydrothermal source. In addition, diagenetic and epigenetic processes may also have played an important role in the manganese mineralization.

Key words: manganese, geochemistry, hydrogenetic, hydrothermal, Yozgat (Turkey).

INTRODUCTION

Manganese oxide deposits are found within several tectonic settings. Based on their mineralogical characteristics and tectonic settings these deposits are classified into hydrogenetic, hydrothermal and diagenetic types (Roy, 1992; Hein et al., 1997). Some parameters such as terrestrial input and microbial processes are important geochemical features regarding the genesis of manganese mineralization (Maynard, 2010; Polgári et al., 2012a, b, 2016). Through supergene processes manganese oxides can be deposited both in marine and terrestrial environments (Maynard, 2010).

Manganese deposits in Turkey are divided into four groups based on their origin, age and structural characteristics (Öztürk, 1993). The first group is manganese deposits of hydrogenetic and hydrothermal type within radiolarian cherts. These are represented by high Mn-Si and low Al-Fe compositions.

Palaeotethys units are exposed in the ophiolites of Karakaya, İzmir–Ankara–Erzincan and Southeastern Anatolia Suture Belts (Fig. 1). Deposits of the second group are associated with black shales within lower Cretaceous carbonates in the western Taurides. The Fe content of these diagenetic deposits is greater than that of those associated with black shales while their Si content is lower. The third group comprises hydrothermal deposits within volcano-sedimentary units of the Black Sea and associated continental arc. The fourth group are formed within Oligocene deposits of the Thrace basin. These deposits with low Mn-Si contents are of high tonnage (Öztürk, 1993).

The manganese mineralization in the study area is exposed throughout the Artova ophiolitic belt NE–NW of the Yozgat district at the base of the northern branch of the Neotethys along the İzmir–Ankara–Erzincan (IAE) Suture Zone (Figs. 1A and 2). Several studies have been conducted regarding the general geology, stratigraphy and tectonics of the region as well as the mineralogy, geochemistry and origin of the manganese mineralizations (Akçe and Kadıoğlu, 2005; Şaşmaz et al., 2005; Kadıoğlu et al., 2006; Öksüz, 2011a, b; Öksüz and Okuyucu, 2014). The mineralization in the study area is associated with the radiolarian cherts included in the Upper Cretaceous ophiolite units. This study: (1) determines the differences and similarities between the types of mineralization by comparing
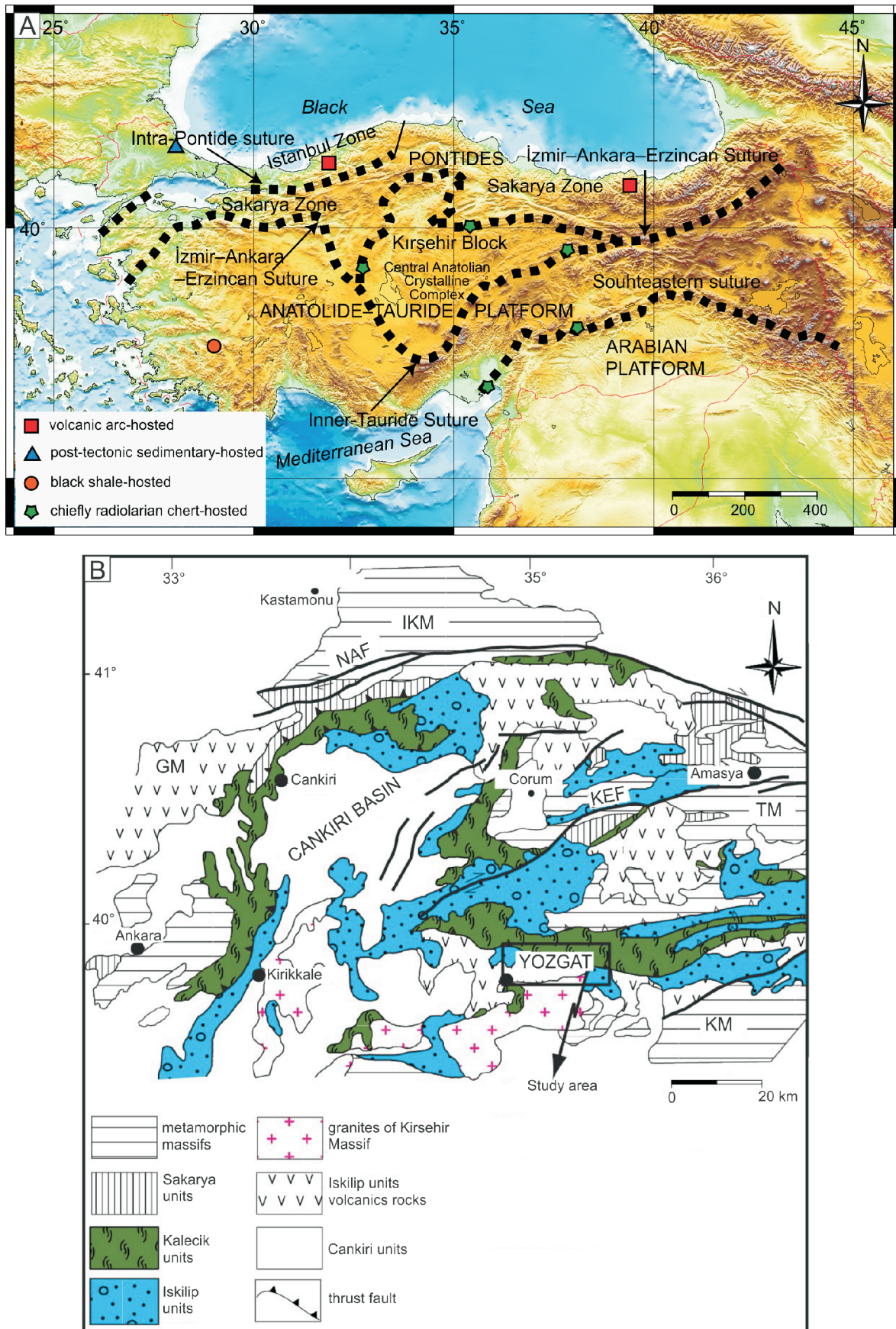
Fig. 1A – map showing major tectonic elements of Turkey, striped lines represent suture zones (modified from Okay and Tüysüz, 1999); B – simplified geological of the Cankiri Basin and surrounding area (modified from by Tüysüz and Dellaloğlu, 1992)

Metamorphic massifs: IKM – Ilgaz–Kargi Massif, TK – Tokat Massif, GM – Galatya Massif, KM – Kirsehir Massif; NAF – North Anatolia Fault, KEF – Kirikkale–Erba Fault
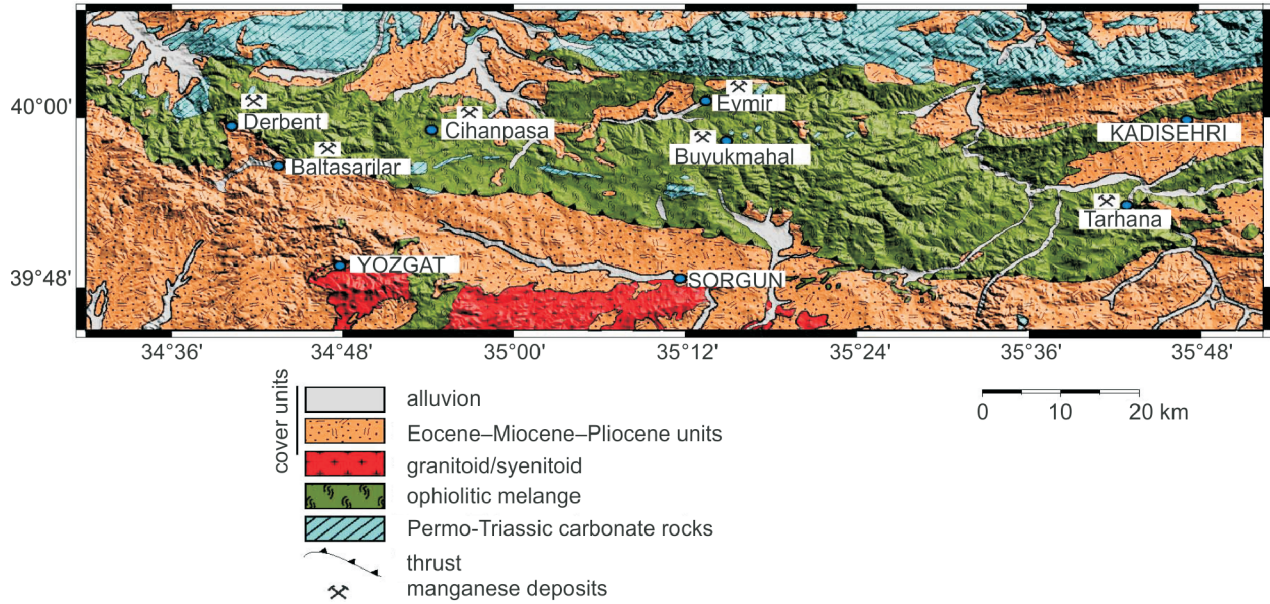
Fig. 2. Geological map of the study area (modified by Ozcan et al., 1980)

their mineralogical, original and geochemical compositions; and (2) develops a tectonic model for the mineralization.

GEOLOGICAL SETTING

Geologically, Turkey is divided into three tectonic units: the Pontides, the Anatolide-Tauride and the Arabian Platform (Ketin, 1966; Okay, 2008; Fig. 1). These units, which were surrounded by oceans during the late Mesozoic, are now separated by tectonic lines or zones where oceans were subducted (Okay, 2008). The Pontides are located north of the northern branch of the Neotethys. Complete closure of this ocean formed the İzmir–Ankara–Erzincan (IAE) Suture. The IAE separates the Pontides in the north from the Anatolides–Taurides in the south. The northern and southern parts of the Kirsehir block are demarcated by the IAE Suture and Inner Tauride Suture, respectively. This block comprises the Kirsehir, Nigde and Akdağ massifs and several basins. The Kirsehir block is also known as the Central Anatolian Crystalline Complex (CACC). The Anatolide–Tauride continent that comprises the CACC was a "foot wall" throughout the Late Cretaceous and large ophiolite masses and ophiolitic melange at its base gave rise to the emplacement of tectonic slices (Fig. 1A). The geological units in the study area are composed of alternations of ophiolitic melange and ophiolitic block, and slice-bearing volcanic and sedimentary deposits which are overlain by a regressive clastic sequence, termed the "Kalecik Unit" (Tüysüz and Dellaloğlu, 1992; Fig. 1B). This unit, at the eastern, western and northern parts of the Çankırı Basin, is recognized as a tectonic slice between the overlying Karakaya and Sakarya units and the underlying Iskilip Unit. The part of the Kalecik Unit in the study area and ophiolitic rocks exposed along the IAE Suture was named the Artova Ophiolitic Complex (AOC) by (Ozcan et al., 1980). The ophiolitic melange is a kind of tectonic complex consisting of rocks of the northern branch of the Neotethys (Şengör and Yılmaz, 1981) that was northerly subducted during the Late Cretaceous, and various rock units from the continental margin (Temiz et al., 2010).

GEOLOGY OF THE STUDY AREA

Units in the study area are categorized into four groups: (1) Permo-Triassic carbonate units, (2) ophiolitic melange (3) intrusives cutting these units and (4) sedimentary and volcanic rocks of Cenozoic basins, known as the Central Anatolian basins, which overlie all these units (Fig. 2). The northern section of the area comprises Permo-Triassic carbonate units. They have a block-like structure in part and are associated with volcanic rocks. The ophiolitic melange is found in the central part of the study area. The emplacement of these ophiolitic rocks is reported to be related to an ensimatic arc (Yalınız et al., 1996) and they are suggested to be the remnants of the northern Neotethys Ocean (Şengör and Yılmaz, 1981). Ophiolitic rocks are recognized as either fragmented ophiolite bodies or ophiolitic melange fragments of various sizes that were formed in front of ophiolite nappe. The CACC is intruded by several granitoid and syenitoid plutons. Plutons at south of the study area cut the ophiolitic and metamorphic units. ^{40}Ar-^{39}Ar biotite and hornblende, titanite and zircon ages of these rocks are reported to be 95–70 Ma (Whitney et al., 2003; Köksal et al., 2004; Boztuğ et al., 2007). These units are overlain by sedimentary and volcanic units deposited in Eocene–Miocene and Pliocene times. The cover units are composed of terrestrial clastic rocks, carbonates, basalt and andesite.

MANGANESE MINERALIZATION

Six different instances of manganese mineralization were investigated in the area described, namely those of: Derbent, Baltasarilar, Cihanpasa, Buyukmahal, Eymir and Tarhana (Fig. 2). These mineralization examples experienced intense tectonism and all of them are interlayered with laminated and/or lenticular radiolarites (Fig. 3A–C). Both radiolarites and mineralization are fractured and folded (Fig. 3A, B). In all these instances, syngenetic type pyrolusite is the main ore mineral. However, in some of them diagenetic and epigenetic pyrolusite and other oxide mineralization are also observed (discussed
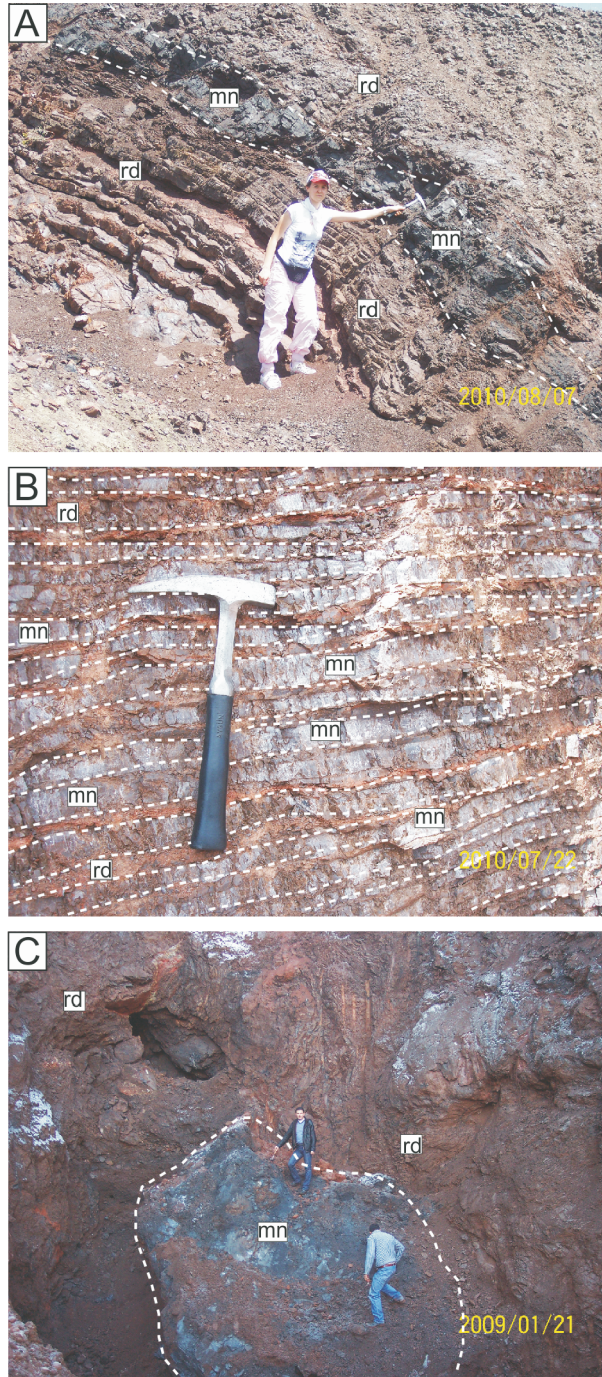
Fig. 3. Laminated, banded and lenticular ore bodies in the study area

A – Buyukmahal mineralization; **B** – Derbent mineralization; **C** – Eymir mineralization; mn – manganese, rd– radiolarite

below). Quartz is the most abundant gangue mineral. In ore microscopy studies, the presence of radiolarian tests and fine-grained pyrolusite is attributed to rapid deposition from fluids (Fig. 4A; Zarasvandi et al., 2016). In addition, pyrolusite veins of various sizes with radiolarite layers and fracture-filling structures are evidence of late-stage mineralization (Zarasvandi et al., 2016).

DERBENT MINERALIZATION

The Derbent manganese mineralization occurs in the western part of the AOC 35 km NW of the Yozgat district (Fig. 2).

The region shows evidence of tectonism, the mineralization and the radiolarite units containing it showing a fractured and folded structure. The strike of the Derbent manganese veins extends discontinuously N–W over 2 km, and dips 10–20°NE and SW. The thickness of the manganese vein zone varies from 10 to 70 cm and the manganese ore is dark red and reddish with a fractured and folded structure. Manganese and iron oxides are the main oxides. In the mineralization, three different mineralization stages-syngenetic, diagenetic and epigenetic were recorded. In the syngenetic stage, typically small euhedral crystals are observed and only pyrolusite (I) was recognized (Fig. 4A). The diagenetic stage is represented by re-mobilization of ore minerals and is characterized by diagenetic manganite and goethite (Fig. 4B, C). The epigenetic stage is represented by post- depositional supergene enrichment and is characterized by fracture-filling pyroluusite (II) (Fig. 4D). Tat Derbent manganese mineralization has been suggested to be of hydrothermal exhalative type (Öksüz, 2011b).

BALTASARILAR MINERALIZATION

The Baltasarilar manganese mineralization is located 25 km NW of Yozgat district (Fig. 2). The mineralization is composed chiefly of manganese oxides and lesser amounts of iron oxide and it occurs within radiolarites as bands and laminae of thickness not exceeding 10 cm. The strike of the Baltasarilar manganese veins extends discontinuously N–W over 5 m, and dips 20°SW. The manganese ore is dark red and reddish and fractured and folded structure. Like in the Derbent region, the mineralization is syngenetic, diagenetic and epigenetic. Based on this, two different pyrolusite types are observed. The pyrolusite may be fine-grained, partly euhedral syngenetic (I) or post-depositional, fracture-filling epigenetic (II) (Fig. 4D). Goethite is diagenetically formed by the alteration of pyrolusite (Fig. 4E).

CIHANPASA MINERALIZATION

The Cihanpasa manganese mineralization is located 30 km N of Yozgat district (Fig. 2). The mineralization is solely composed of syngenetic pyrolusite. As in the other mineralization instances, it is intensely folded and fractured. The strike of the Cihanpaşa manganese veins extends discontinuously N–W over 3 m, and dips 10°SW. The thickness of the manganese vein zone varies from 3 to 8 cm and the manganese ore is dark red and reddish and fractured and folded.

BUYUKMAHAL MINERALIZATION

The Buyukmahal area is situated 35 km NE of the Yozgat district (Fig. 2). The mineralization is composed of syngenetic pyrolusite and diagenetic magnetite. Although volcanic units are exposed in the region, the mineralization occurs within the radiolarites as bands and lenses. As in the other mineralization instances, it is intensely folded and fractured. The strike of the manganese veins extends discontinuously N–W and NE over 20 m, and dips 55–25°NE and NW. The thickness of the manganese vein zone varies from 50 to 60 cm and the manganese ore is dark red and reddish and fractured and folded.

EYMIR MINERALIZATION

The Eymir mineralization, 80 km NE of the Yozgat district, is the largest manganese occurrence in the region (Fig. 2). The mineralization has been exploited by various companies, although not currently. It occurs as thin and thick bands and lenses. The mineralization, formed in syngenetic, diagenetic and epigenetic stages, contains iron and manganese oxide minerals. The region has experienced intense tectonism, with
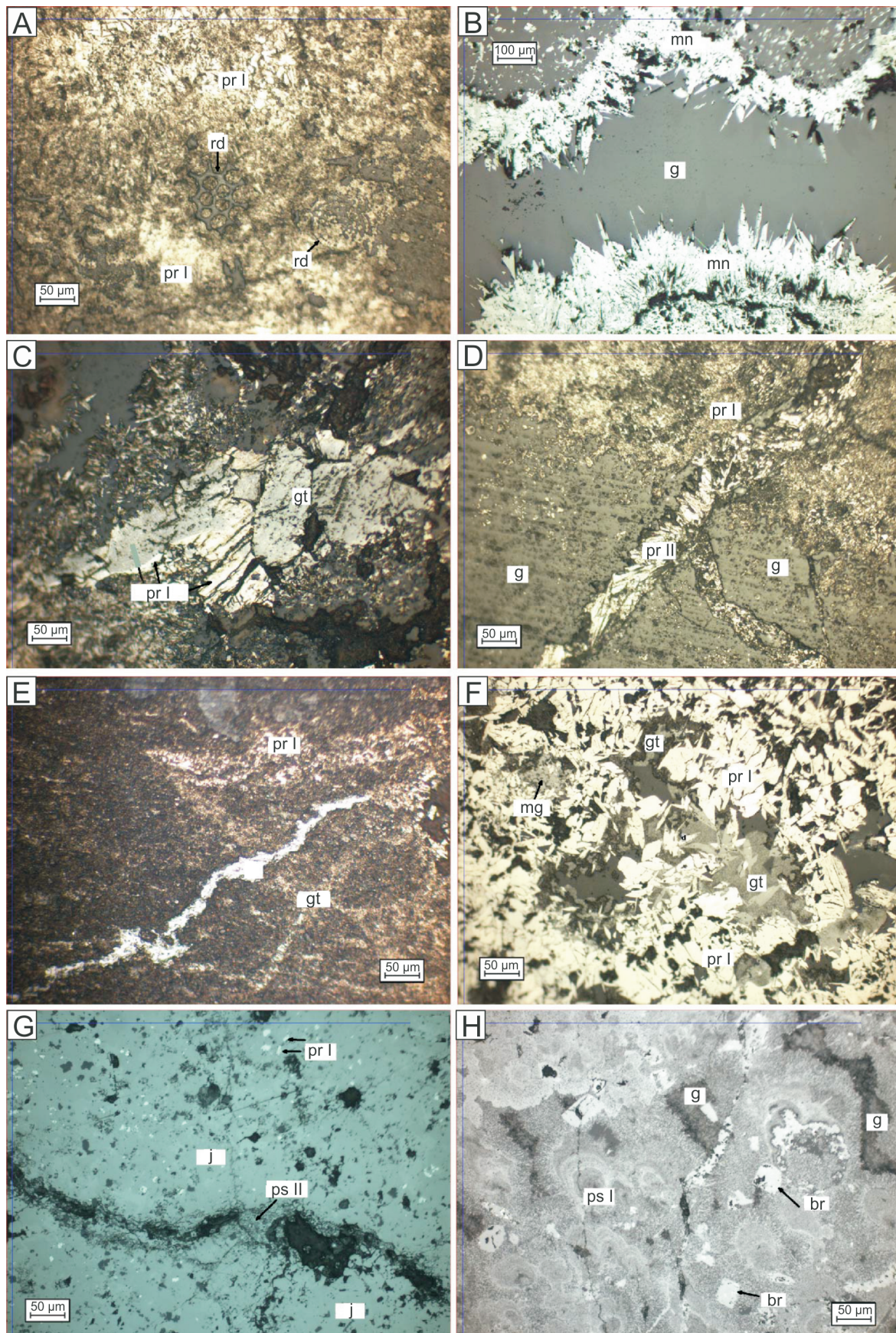
Fig. 4A – ore microscopy view of fossil radiolaria and fine-grained euhedral pyrolusite (pr I) // nicol; **B** – manganite (mn) // nicol; **C** – goethite (gt) and pyrolusite (pr I) // nicol; **D** – fine-grained pyrolusite (pr I), fracture-filling pyrolusite (pr II) and gangue (g) // nicol; **E** – goethite (gt) as a product transformation from pyrolusite and fine-grained pyrolusite (pr I) // nicol; **F** – euhedral pyrolusite (pr I) and diagenetic goethite (gt), magnetite (mg) // nicol; **G** – fracture-filling psilomelane (ps II), euhedral pyrolusite (pr I) and diagenetic jacobsite // nicol; **H** – psilomelane (ps I), diagenetic braunite (br) and gangue (g) // nicol

folding and fracturing. Ore minerals are associated with extremely folded and fractured radiolarites. The strike of the Eymir manganese veins extends discontinuously N–W over 3 km, and dips 20–25°SW and SE. The thickness of the manganese vein zone varies from 1 to 10 m and the manganese ore is dark red and reddish and fractured and folded (Fig. 3C). Euhedral pyrolusite is thought to have been formed syngenetically (Fig. 4F, G). Psilomelane is observed as both syngenetic [psilomelan(I)] (Fig. 4H) and epigenetic types [psilomelan(II)] (Fig. 4G). In addition, diagenetic magnetite, goethite, jacobsite and braunite are also recognized (Fig. 4F–H).

TARHANA MINERALIZATION

In the Tarhana region, 120 km east of the Yozgat district, syngenetic manganese oxide mineralization occurs (Fig. 2). Ore paragenesis is solely composed of pyrolusite and quartz is the main gangue mineral. The strike of the Tarhana manganese veins extends discontinuously N–W over 10 m, and dips 10–20°NE and SW. The thickness of the manganese vein zone varies from 10 to 15 cm and the manganese ore is dark red and reddish and fractured and folded.

ANALYTICAL PROCEDURES

Fifty 500 g ore samples were collected from the Derbent, Baltasarilar, Cihanpasa, Buyukmahal, Eymir and Tarhana manganese mineralization occurrences, with systematic sampling from top to bottom of the ore. Samples were taken at 30 cm intervals. Powders of 12 samples (<200 mesh) were analysed at ACME Laboratories (CANADA). Major oxide and trace element contents were determined by ICP-ES and REEs were analysed by ICP-MS. 30 g samples were powdered to 100 µm for geochemical analysis. 0.5 g samples were processed in HCl-HNO$_3$-H$_2$O solution at ~95°C for 1 hour and then the amount of each sample was increased to 10 ml for the final filtering. Analytical results are given in Appendices 1 to 3*. In addition, in order to determine the paragenesis and textural characteristics of the mineralization, 40 polished sections were studied by ore microscopy. XRD analysis of twenty samples was done at TPAO (Turkish Petroleum Corporation) laboratories. A Rigaku DMAX IIIC model X-ray diffractometer with a Cu target (2–70° 2) was used in the analyses. Ore minerals were also studied with a *Thermo Scientific DXR Raman Microscope* at the Geological Engineering Department of Ankara University. The Raman spectra obtained were evaluated with the Crystal Sleuth program to determine the mineral paragenesis. Chemical compositions of some ore minerals (manganite, psilomelane, pyrolusite, braunite) were determined by microprobe analysis (EPMA) conducted at Montan University in Leoben (Austria).

RESULTS

GEOCHEMISTRY

The main, trace and REE contents of 50 ore samples collected from the mineralization occurrences studied in the AOC are given in Appendices 1, 2 and 3. Major oxide and some trace element data on manganese mineralization of different origins are shown in Table 1. REE contents of samples from similar and different types of manganese mineralization are given in Table 2.

MAJOR AND TRACE ELEMENTS GEOCHEMISTRY

Major and trace element concentrations and their associations are commonly used to analyse manganese and ferromanganese deposits (Öksüz, 2011b; Polgári et al., 2012b; Zarasvandi et al., 2013). Mn contents of ore samples from the AOC are 5.62–62.86 wt.% (*n* = 50 samples; average 46.76 wt.%) and Fe concentrations are 0.03–31.11 wt.% (average 2.83 wt.%; Appendix 1).

SiO$_2$ contents of the samples studied are 1.76–55.92 wt.% (average 17.24 wt.%; Appendix 1). Although Co/Zn ratios of all samples are >0.15, the ratios of the Baltasarilar and Cihanpasa samples in particular are <2.5. Co/Zn ratios in other regions are very close to 2.5 or higher (Appendix 1) indicating that a hydrogenetic process was involved in the formation of the manganese oxide mineralization in the AOC. If Co/Ni <1, the deposit has a sedimentary origin (Fernandez and Moro, 1998) while Co/Ni >1 indicates a marine environment (Delian, 1994). Likewise, Co/Ni is <1 for the Baltasarilar and Cihanpasa samples and it is <1 for other mineralization instances. These data imply that mineralization in the area is of an exhalative sedimentary type. Co is a notable bioessential element (Moffett and Ho, 1996; Polgári et al., 2012b). This feature of cobalt can be considered as evidence for subsequent selective enrichment of bioessential elements in AOC Mn oxides and their formation via microbial processes (Zarasvandi et al., 2016).

As, Ba, Cu, Li, Mo, Pb, Sb, Sr, V and Zn contents are enriched in hydrothermal fluids (Nicholson, 1992a). Concentrations of As, Ba, Cu, Pb, Sr, V and Zn tend to be enriched in all mineralization examples in the area studied (Appendix 2). In hydrothermal systems, Zn concentration is expected to be fractionated in proximal sulphide deposits (Hein et al., 2008). Zn concentrations of the mneralization studied in the AOC are 35–407 ppm (average 113.6 ppm) which may be attributed to leaching from sulphide mineralization at depth (Appendix 2; Şaşmaz et al., 2014). High Ni and Cr contents could be explained by leaching from ultramafic rocks or contributions from ultramafic clastic material (Hein et al., 2008). Ni may also occur in sulphide zones and therefore high Ni concentrations may indicate multiple sources. If high Ni concentrations are not correlated with high Cr contents, ultramafic material may not be the source (Hein et al., 2008). However, when concentrations of these elements are high and if Ni content is relatively lower than Cr, leaching from ultramafic rocks might be plausible (Şaşmaz et al., 2014). Ni concentrations in the samples are 38.0–950.9 ppm (average 204.8 ppm) and Cr concentrations are 13.68–2737.0 ppm (average 155.59 ppm; Appendix 1). These results show that the mineralization in the study area is probably associated with leaching from ultramafic rocks.

According to Hein et al. (2008), high Cu, Zn, Pb and Cd contents typically reflect the effect of sulphides. Cu and Pb enrichment in the samples studied may indicate leaching from sulphide at depth (27.13–1606.5 ppm, average 274.3 ppm and 0.1–147.8 ppm, average 18.9 ppm, respectively; Appendix 2; Şaşmaz et al., 2014). Low Mn contents in ferromanganese ores are indicative of low-temperature hydrothermal solutions (Hein et al., 2008; Şaşmaz et al., 2014). The Mn concentrations of the samples are 3.7–198.2 ppm (average 38.8 ppm) implying the involvement of low-temperature hydrothermal fluids (Appendix 2). Co contents in hydrothermal deposits is lower than those

---

T a b l e 1

Major and trace element contents of various types of manganese deposit

Number of samples	7	28	22	9	11	7	13	23	10	17	4	4	5	15	5
Countries	China	Pakistan	Pakistan	Northeast Pacific Ocean	Iran	Turkey	Turkey Ophiolitic Melange								
Regions	Guichi (1)	Waziristan (2)	Hazara (3)	Baby Bare (4)	Kermanshah Ophiolite Sorkhvand (5)	Ulukent (6)	Maden Complex (7)	Cayirli (8)	Kasimaga (9)	D	B	C	BM	E	T
Origin	sedimentary	volcano-sedimentary	hydrothermal-hydrogenous	hydrothermal	hydrothermal	sedimentary	sedimentary/diagenetic	volcano-sedimentary	volcano-sedimentary						
SiO_2 [%]	(-)	43.69	9.41	2.02*	40.82	13.68	24.17	63.02	13.43	6.34	20.55	44.64	23.42	14.25	35.90
Al_2O_3 [%]	(-)	0.73	12.53	0.27*	0.48	2.49	4.58	0.65	2.95	0.33	0.88	2.98	4.33	0.80	0.52
Fe_2O_3 [%]	(-)	2.96	20.33	2.30*	2.29	3.72	34.07	0.68	14.33	0.75	0.35	26.18	7.02	0.26	0.05
MgO [%]	(-)	0.60	0.59	1.58*	0.05	1.99	1.15	0.20	12.72	0.43	0.38	0.59	2.11	0.63	0.38
CaO [%]	(-)	1.28	6.43	0.97*	0.52	4.05	9.24	0.24	6.82	2.48	1.56	4.14	5.08	2.56	0.29
Na_2O [%]	(-)	0.29	0.07	0.64*	0.03	0.24	0.07	0.05	0.06	0.04	0.05	0.11	0.23	0.01	0.02
K_2O [%]	(-)	0.22	0.88	0.22*	0.06	0.05	0.05	0.11	0.19	0.63	1.25	0.37	0.58	0.03	0.43
TiO_2 [%]	(-)	0.32	0.84	0.04*	0.03	0.10	0.17	0.03	0.10	0.01	0.02	0.14	0.19	0.02	0.01
P_2O_5 [%]	(-)	0.25	3.73	0.04*	0.06	0.18	0.94	0.04	0.08	0.07	0.03	0.49	0.14	0.07	0.08
MnO [%]	(-)	45.88	33.78	48.52*	39.52	63.78	18.70	29.22	40.43	68.53	60.82	11.33	44.83	73.77	53.30
Ba [ppm]	212.56	415.00	6304	7091.67	1038.34	427.00	1503.50	1229.40	2719.40	10876.6	15508.8	893.0	6278.8	2588.1	2720.3
V [ppm]	167.86	144.00	573	172.33	30.68	(-)	699.41	143.70	106.10	139.6	167.3	415.8	416.6	131.6	204.8
Cr [ppm]	107.21	46.00	247	8.89	(-)	(-)	20.50	13.70	10.00	220.16	121.45	13.68	24.63	34.67	570.66
Co [ppm]	4.77	11.00	404	135.33	33.35	13.00	66.56	25.21	49.50	367.6	159.6	106.1	621.5	104.0	333.4
Ni [ppm]	89.39	36.00	305	300.67	98.61	10.00	735.27	69.40	23.00	234.6	358.3	390.5	266.1	72.4	100.9
Cu [ppm]	31.03	72.00	375	226.00	161.18	56.00	434.14	154.90	126.80	180.5	92.8	652.0	426.9	90.2	992.8
oZn [ppm]	137.36	64.00	580	123.22	64.12	70.00	284.01	66.70	63.50	94.8	121.3	328.3	129.4	66.7	72.8
Pb [ppm]	16.49	49.00	2357	(-)	6.56	65.00	133.93	6.50	53.50	1.3	5.7	133.9	30.5	9.9	15.9
Th [ppm]	(-)	2.00	31	1.00	0.28	(-)	2.48	0.40	433.20	0.2	0.5	3.2	3.7	0.6	0.2
Sr [ppm]	741.34	(-)	(-)	877.44	667.65	185.00	1409.10	243.40	255.00	3035.0	3838.2	303.3	764.4	115.1	1478.8
Nb [ppm]	6.70	(-)	(-)	1.50	0.27	(-)	5.20	0.70	11.10	0.1	0.1	4.2	2.5	0.1	0.3
Zr [ppm]	(-)	(-)	(-)	9.22	5.87	(-)	89.99	4.00	26.90	16.1	9.8	99.1	58.4	8.9	2.5
Co/Ni	0.05	0.31	1.32	0.45	0.50	1.30	0.09	0.36	2.15	2.6	0.4	0.3	2.4	2.0	3.5
Co/Zn	0.03	0.17	0.70	1.10	0.81	0.19	0.24	0.38	0.78	4.3	1.4	0.3	4.9	2.3	4.6
Mn/Fe	(-)	199.00	2.16	26.89	127.30	18.98	0.61	97.17	12.02	902.65	612.53	0.57	9.61	1053.13	1332.39

Analyses taken from (1) Xie et al. (2006); (2 and 3) Shah and Moon (2007); (4) Filtzgerald et al. (2006); (5) Zarasvandi et al. (2016); (6) Öztürk (1993); (7) Şaşmaz et al. (2014); (8) Karakuş et al. (2010); (9) Koç et al. (2000); * – values are from element type; D – Derbent, B – Baltasarilar; C – Cihanpasa; BM – Buyukmahal; E – Eymir; T – Tarhana; (-) there is no analysis

T a b l e   2

REE concentrations [ppm] of hydrogenous and hydrothermal manganese oxide deposits from different localities

	La	Ce	Pr	Nd	Sm	Eu	Gd	Tb	Dy	Ho	Er	Tm	Yb	Lu	REE
Hydrogeneous deposits															
Johnson Island (Wiltshire et al., 1999)	260.00	1201.00	44.80	192.70	35.40	10.10	48.50	6.80	43.70	9.90	28.90	4.30	27.90	3.60	1917.70
Indian Ocean (Nath et al., 1992)	153.40	714.10	34.80	142.00	33.80	8.90	43.70	5.70	30.60	5.60	15.50	2.30	15.00	2.20	1207.60
Pitcairn Island hotspot (Glasby et al., 1997)	276.80	741.70	50.80	214.40	42.70	10.20	49.90	7.20	44.70	9.20	26.40	3.90	26.00	4.00	1508.10
Hydrothermal deposits															
Neptune Deposit (Del Rio Salas, 2008)	125.20	289.30	24.40	78.70	12.80	7.20	10.30	1.30	6.60	1.10	3.10	0.30	2.30	0.30	563.10
Baleo deposit (Del Rio Salas, 2008)	118.60	190.30	5.40	28.40	7.80	0.10	5.80	0.90	7.50	1.60	6.00	0.70	6.10	0.80	379.80
Mn mineralization of Upenninine Ophiolite, Italy (Robertson and Fleet, 1976)	1.70	5.00		2.70	0.70	0.20	(-)	(-)	(-)	(-)	(-)	(-)	0.20	1.80	12.30
Manganese samples of Baft Ophiolite Area (Heshmatbehzadi et al., 2010)	11.10	9.90	4.20	7.60	1.60	0.62	1.90	0.88	0.70	1.10	1.35	0.42	1.15	0.16	42.68
Kermanshah Ophiolitic Melange Sorkhvand manganese deposit (Zarasvandi et al., 2016)	4.80	7.45	0.87	3.18	0.62	0.15	0.70	0.13	0.84	0.19	0.62	0.10	0.79	0.14	19.61
Maden Complex Ferromanganese deposits (Sasmaz et al., 2014)	158.03	48.24	36.11	147.98	27.14	6.81	29.93	4.84	25.38	4.86	13.93	1.80	11.31	1.59	517.86
Artova Ophiolitic Complex															
Derbent (this study)	8.25	5.34	1.58	6.72	1.42	0.54	1.95	0.33	2.04	0.50	1.51	0.24	1.53	0.25	32.20
Baltasarılar (this study)	8.00	10.53	1.84	7.40	1.46	0.35	1.31	0.22	1.14	0.26	0.74	0.12	0.83	0.15	34.33
Cihanpaşa (this study)	103.55	53.03	27.33	113.40	21.74	4.97	20.07	3.02	16.46	3.09	8.53	1.23	8.09	1.15	385.66
Buyukmahal (this study)	35.30	33.50	8.36	34.22	6.54	1.57	6.49	1.04	6.08	1.24	3.73	0.56	3.58	0.54	142.75
Eymir (this study)	5.92	16.21	1.39	5.74	1.14	0.28	1.24	0.21	1.21	0.26	0.79	0.12	0.78	0.12	35.41
Tarhana (this study)	14.38	17.28	2.38	9.12	1.63	0.51	1.48	0.25	1.38	0.28	0.85	0.16	1.10	0.17	50.98

The table also includes those of the AOC manganese deposits
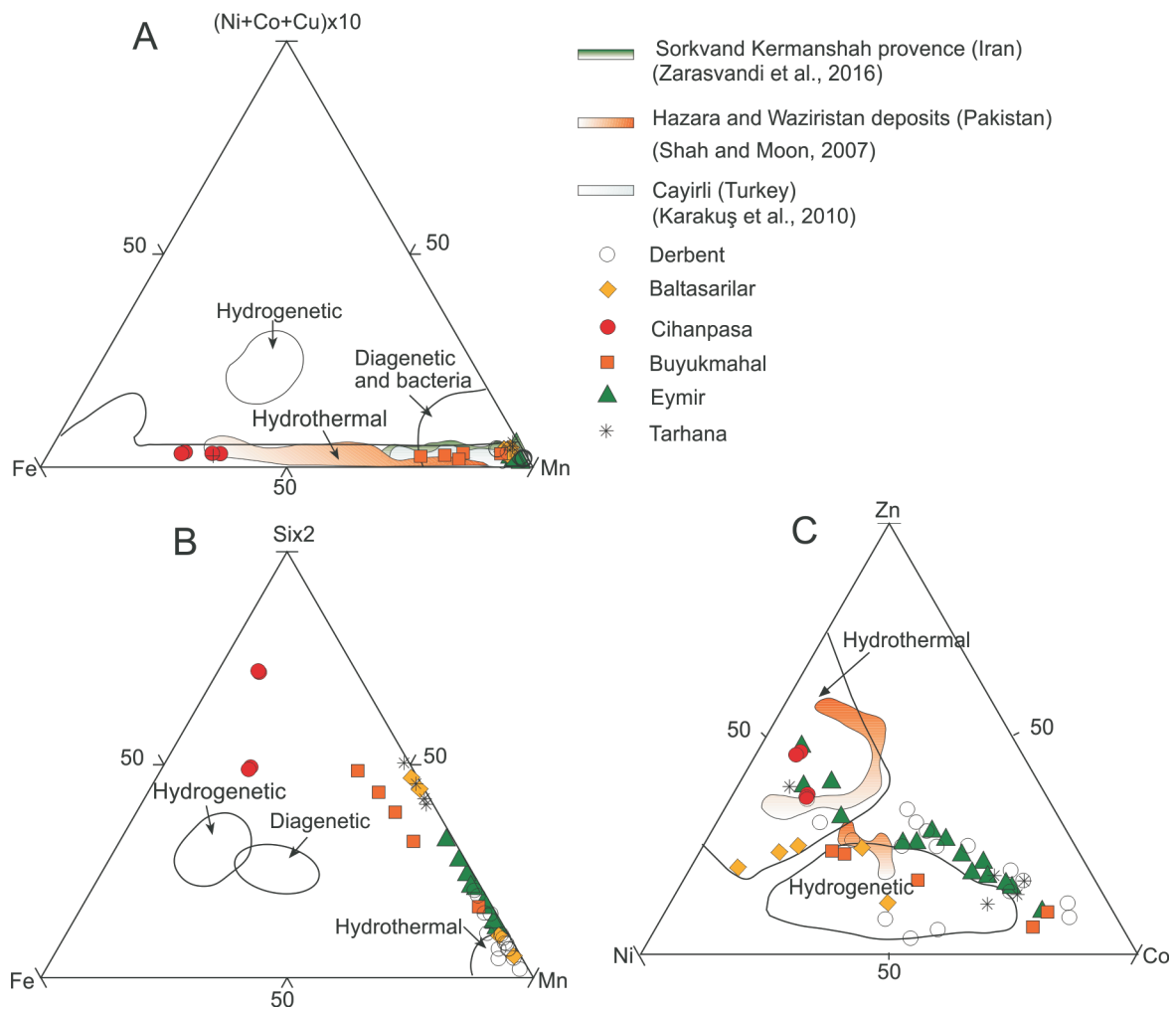
**Fig. 5A – Fe-(Ni+Co+Cu) 10Mn discrimination diagram (Bonatti et al., 1972; Crerar et al., 1982; Hein et al., 1992);
B – Fe-Si 2Mn diagram (Toth, 1980); C – Ni-Zn-Co diagram (Choi and Hariya, 1992)**

in hydrogenetic deposits and therefore high Co concentrations reflect deep marine environments (Del Rio Salas et al., 2008). Co concentrations of the manganese mineralization in the AOC are 27.2 to 1432.1 ppm (average 268.1 ppm) which are relatively high, reflecting a hydrogenetic contribution (Appendix 2). According to Hein et al. (2008), high Ba and low Fe, Co, Ni, Cu and Zn contents of manganese oxides may indicate leaching from organic-rich sediments or insufficient barite dissolution at depth. Due to sedimentation and volcanic activity effects, Ba concentrations in hydrothermal fluids are greater than in seawater (Monnin et al., 2001; Öksüz, 2011a). Ba concentrations in the manganese mineralization of the AOC are 91.0–37137.0 ppm (average 6807.7 ppm; Appendix 2). Based on these high Ba contents, mineralization in the study area reflects a hydrothermal origin. High arsenic contents are indicative of sediment input to the hydrothermal manganese formation (Nicholson, 1992a, b). Arsenic concentrations in the samples are 5.9–199.9 ppm (average 46.3 ppm; Appendix 2). This enrichment might indicate the role of hydrothermal fluids (Şaşmaz et al., 2014).

Trace element concentrations (As, Cu, Ni, Pb and Zn) in the AOC samples are lower than those of hydrogenetic deposits but significantly higher than those of hydrothermal deposits (Appendix 2). Al and Ti concentrations are also used for description

of manganese mineralization and Al is generally associated with clay minerals in sediments (Crerar et al., 1982). Ti is immobile in hydrothermal solutions and it defines the rate of clastic input (Sugisaki, 1984). High Al contents in manganese oxide deposits are an important indicator of sedimentary input during sedimentation (Choi and Hariya, 1992). Al concentrations in the AOC samples are 0.01–3.19 wt.% (average 0.61 wt.%) and Ti concentrations are 0.01–0.17 wt.% (average 0.03 wt.%; Appendix 1). Relatively high Al concentrations in the AOC ores may have been derived from the radiolarite. Low Ti contents might indicate limited clastic input during deposition (Şaşmaz et al., 2014).

Various major and trace element diagrams have been used for discrimination of manganese deposits of different origins (Bonatti et al., 1972; Toth, 1980; Crerar et al., 1982; Adachi et al., 1986; Peters, 1988; Choi and Hariya, 1992; Nicholson, 1992a; Shah and Moon, 2007). These diagrams are useful for distinguishing hydrothermal (terrestrial or marine) versus hydrogenetic origins. The term hydrothermal has been used for sedimentary-exhalative manganese mineralization or for pools in terrestrial environments and manganese oxides deposited directly from hot springs in geothermal systems (Nicholson, 1992a). The term hydrogenetic commonly refers to adsorption of materials dissolved in seawater or deposits that are depos-
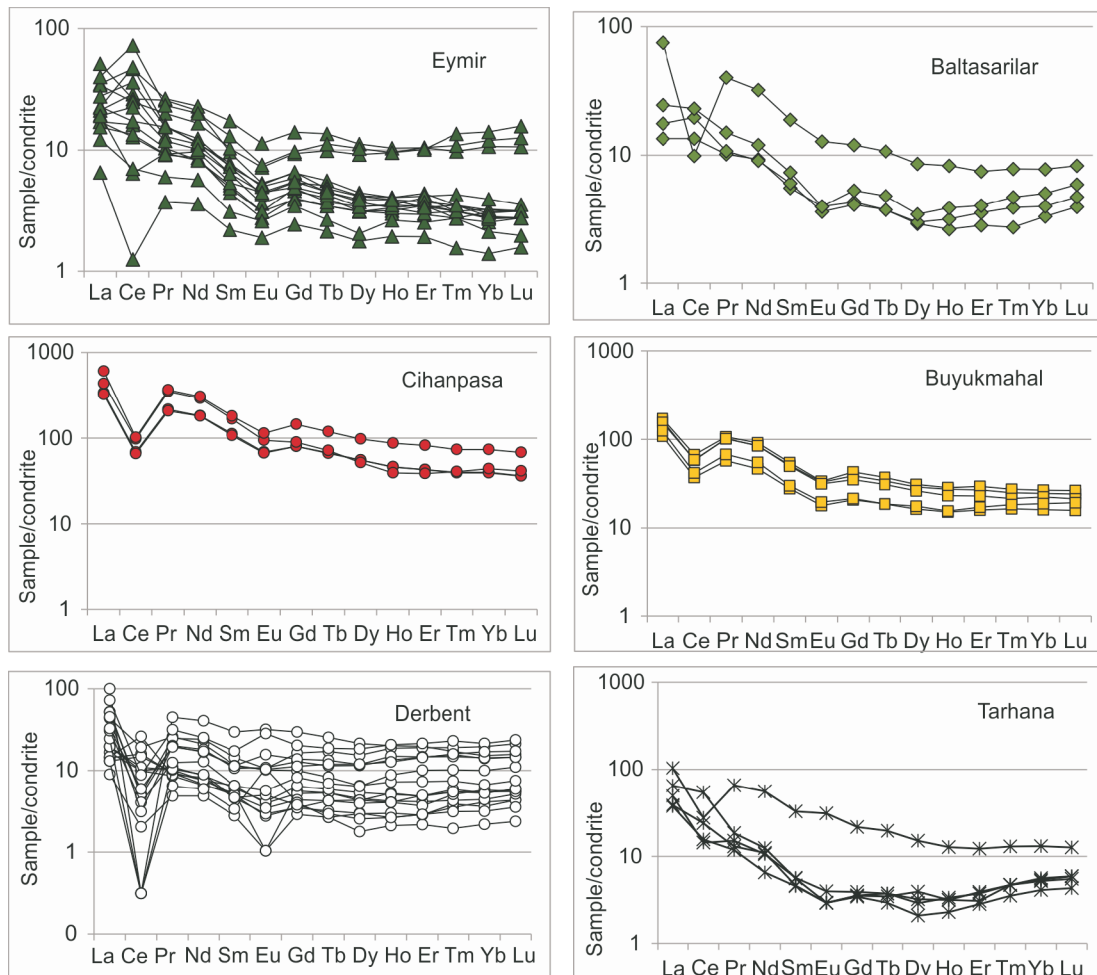
Fig. 6. Chondrite-normalized REE diagram for the ore samples (normalization values after Evensen, 1978)

ited slowly (Bonatti et al., 1972; Crerar et al., 1982; Nicholson, 1992a). In the Fe-(Cu+Ni+Co) 10-Mn triangular diagram, the ore samples studied are compared to samples from other regions associated with ophiolites (Bonatti et al., 1972; Crerar et al., 1982; Hein et al., 1992; Shah and Moon, 2007; Karakuş et al., 2010; Zarasvandi et al., 2016; Fig. 5A). Based on this, all samples plot in the hydrothermal field. In addition, some samples show contribution from diagenetic or microbial processes. In the Fe-Six2-Mn diagram, all Cihanpasa samples are distributed in the hydrogenetic field, while others plot in the vicinity of the hydrothermal field (Toth, 1980; Fig. 5B). In the Ni-Zn-Co diagram, ore samples are compared with samples associated with ophiolites (Choi and Hariya, 1992; Fig. 5C). Based on this diagram, ore samples from the Derbent, Eymir, Buyukmahal and Tarhana areas mostly plot in the hydrogenetic field and the Cihanpasa samples cluster in the hydrothermal field while samples from the Baltasarilar area are distributed in both fields (Choi and Hariya, 1992; Fig. 5C).

Major and trace element contents of various manganese deposits of hydrothermal and hydrogenetic origin in Turkey and worldwide are given in Table 1. Major and trace element concentrations of AOC manganese mineralization are compared with those of Guichi (China), Waziristan, Hazara (Pakistan), Baby Bare (NE Pacific Ocean), and the Sorkhvand (Iran), Ulukent, Maden Complex, Cayirli, Kasimaga (Turkey) deposits (Koç et al., 2000; Fitzgerald and Gillis, 2006; Xie et al., 2006;

Shah and Moon, 2007; Karakuş et al., 2010; Şaşmaz et al., 2014; Zarasvandi et al., 2016; Table 1).

REE GEOCHEMISTRY

Results of REE analysis and some REE ratios of the ore samples studied are given in Appendix 3. In addition, REE contents of various manganese oxide deposits from Turkey and worldwide are compared with those of the samples studied (Table 2). Moreover, chondrite-normalized patterns of the samples are shown in Figure 6. Element variation diagrams for deep marine, MOR hydrothermal, EPR Fe-Mn sediments, Phanerozoic Fe-Mn umbers and hydrogenetic Mn crusts and an element variation diagram constructed using average values of the samples studied are shown in Figure 7.

Examination of the REE geochemistry of ore deposits provides an insight into their origin (Bau and Möller, 1991). Therefore, REE contents of manganese oxide deposits from various regions are compared with those from the study area (Table 2). As shown in Table 2 and Figure 7, REE concentrations of hydrothermal deposits are lower than those of hydrogenetic deposits (Hein et al., 1990; Usui and Someya, 1997; Kato et al., 2011). Total REE (SREE) contents of hydrothermal occurrences vary widely (Mills et al., 2001). REE content of the AOC samples is 6.68–518.27 ppm (average 74.54 ppm). Although these values are higher than for the Cihanpasa and
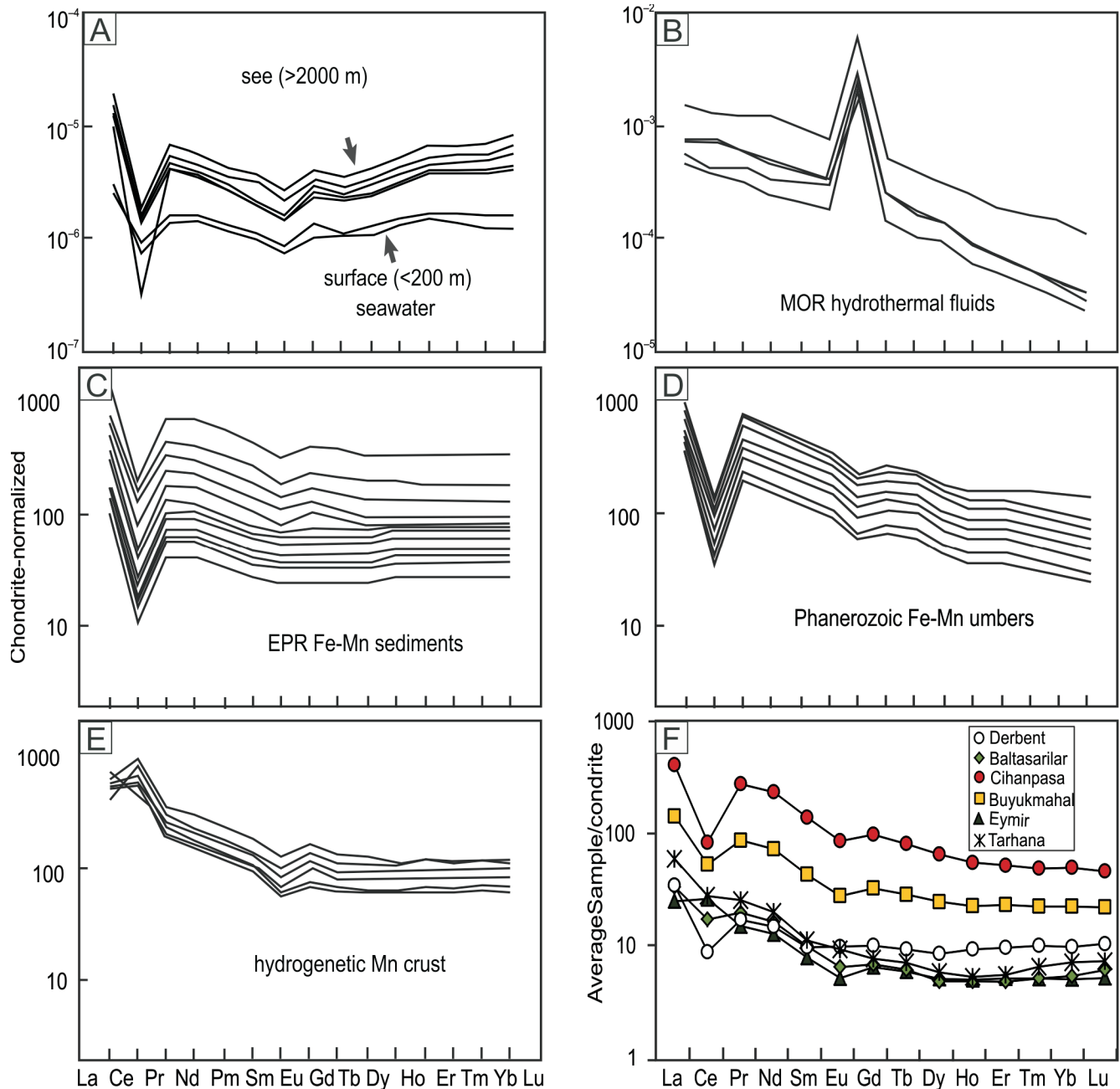
Fig. 7A – chondrite-normalized REE patterns of modern seawater; B – MOR hydrothermal fluids; C – EPR (East Pacific Rise) hydrothermal Fe-Mn sediments; D – Phanerozoic hydrothermal Fe-Mn umbers; E – hydrogenetic Mn crusts (Kato et al., 2006); F – chondrite-normalized REE diagram for average ore samples in the study area (normalization values are from Evensen, 1978)

Buyukmahal areas (305.13–518.27 ppm, average 385.66 ppm and 99.09–178.36 ppm, average 142.75 ppm, respectively), they are generally higher than those of hydrothermal deposits but relatively lower than those of hydrogenetic deposits (Appendix 3 and Table 2). The slight enrichment of REEs in both regions is attributed to the sedimentary cover (Şaşmaz et al., 2014). Chondrite-normalized patterns of the samples are shown in Figure 6. In addition, spider diagrams constructed using average values of the samples are shown in Figure 7. These diagrams are compared with element variation diagrams of similar manganese occurrences in Figure 7. Based on this, the pattern of the ore samples studied greatly resembles those of Phanerozoic Fe-Mn umbers and slightly resembles EPR hydrothermal Fe-Mn sediments and deep-marine examples (Fig. 7A,

C, D). Fractionation from LREE to HREE during the manganese oxidation process can be considered as evidence for primary enrichment of REE (Xie et al., 2006; Şaşmaz et al., 2014). In the samples studied, the LREE/HREE ratio is 1.92–16.89 ppm (average 5.58 ppm) indicating that, since they are more stable, LREEs in hydrothermal solutions are preferably enriched with respect to HREEs (Ruhlin and Owen, 1986; Zarasvandi et al., 2013). Consequently, it can be concluded that hydrothermal solutions played an important role in the formation of the manganese mineralization studied. Y/Ho ratios of the samples are 16.81–51.82 (average 28.90), high Y/Ho ratios indicating multiple sources for the mineralization. In other words, in addition to deep marine conditions, material of terrestrial origin was also incorporated during the mineralization
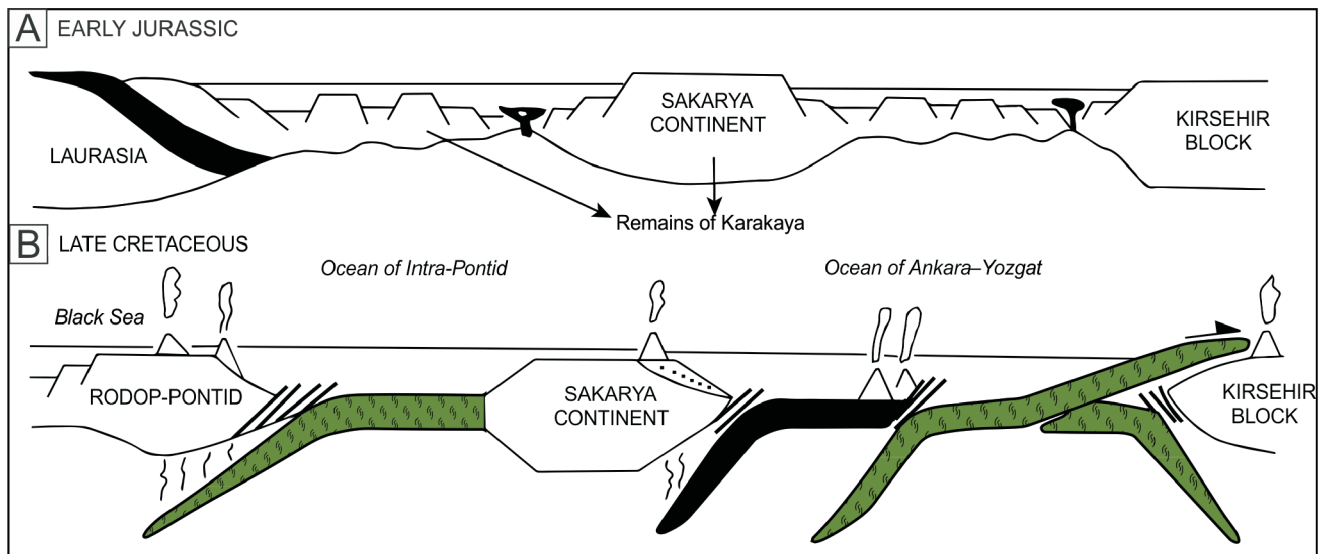
Fig. 8. A sketch model showing the tectonic relation between Permo-Triassic and Lower Paleocene rocks in the Cankiri Basin (Tüysüz and Dellaoğlu, 1992)

(Nayan et al., 1994). LaN/NdN and DyN/YbN ratios are also useful for determination of origin. The LaN/NdN ratio in hydrothermal solutions is 3.0–7.4, with average of 4.5 and the DyN/YbN ratio is 0.6–2.1 with an average of 1.2. These ratios in manganese crusts are 2.7–4.3 and 0.4–1.2 (Fitzgerald and Gillis, 2006). The LaN/NdN and DyN/YbN ratios of the samples studied are 1.45–5.22 (average 2.31) and 0.51–1.41 (average 0.98). These data indicate a hydrothermal source. In normal seawater the Er/Nd ratio is 0.27 (De Baar et al., 1988), but this ratio may be <0.1 due to increasing amounts of detrital material during mineralization, or a concentration of Nd which is more easily concentrated than Er during diagenesis (German and Elderfield, 1989; Bellanca et al., 1997). The Er/Nd ratios of the samples studied are <0.27, except for five samples (D12-13, D15-16-17; 0.05–0.31 and average 0.15). This indicates that the mineralization was accompanied by diagenetic processes, together with a detrital contribution.

Eu and Ce are important elements for determination of the origin and paleoredox potential of the depositional environment (Sabatino et al., 2011). The Ce anomaly is calculated from the equation $Ce^* = Ce_{norm}/[^2/_3La_{norm}+^1/_3Pr_{norm}]$ while the Eu anomaly is computed from the equation $Eu^* = Eu_{norm}/[^2/_3Sm_{norm}+^1/_3Gd_{norm}]$ (Taylor and McLennan, 1985). In these formulae, chondrite-normalized values were used (Evensen et al., 1978). Negative or positive anomalies of these elements may define the origin of formation. For example, a weak negative Ce anomaly indicates volcanic input (Fleet et al., 1976) or volcanic contribution to the seawater. In addition, it may also point to a high growth rate of hydrothermal crusts (Hein et al., 1997). By contrast, a strong negative Ce anomaly characterizes low-temperature hydrothermal deposits of a continental arc in spreading centres and in the vicinity of mid-ocean ridge hot points (Decarlo and Mcmurtry, 1992; Hodkinson et al., 1994). Positive Ce anomalies are characteristic of modern submarine manganese oxyhydroxide deposits and nodules (Kunzendorf and Glasby, 1994). All samples from the Cihanpasa and Buyukmahal areas demonstrate a negative Ce anomaly and resemble low-temperature hydrothermal deposits (Appendix 3 and Fig. 6). Samples from other mineralization occurrences (Derbent, Baltasarilar, Eymir and Tarhana) show both positive and negative Ce anomalies (Appendix 3 and Fig. 6). Based on these results, it can be inferred that both hydrothermal and hydrogenetic processes were effective in the formation of the AOC mineralization (Shah and Moon, 2007). Positive Eu anomalies in hydrothermal deposits are indicative of high-temperature hydrothermal fluids (Michard, 1989) and high Eu concentrations during circulation reflects the interaction between substrate volcanic rocks and hot waters (Usui and Mita, 1995). Negative Eu anomalies indicate relatively little interaction between volcanic rocks and thermal waters (Usui and Mita, 1995). These anomalies also imply crustal contamination and/or sediment contribution (Öksüz, 2011a). Except for some samples from the Derbent area, all other samples from the study area are represented by negative Eu anomalies (Appendix 3 and Fig. 6). Although these values indicate relatively little interaction with volcanic rocks during the mineralization, both positive and negative anomalies were recorded in the Derbent area and show that hydrothermal fluids were involved in hydrothermal mineralization at times, thus increasing the temperature. The negative Eu anomaly might show that the hydrothermal source was in the distal part of the mineralization area or it was greatly mixed with seawater (Sabatino et al., 2011).

Ce_{anom} values ($Ce_{anom} = log[3Ce_N/(2La_N+Nd_N)]$) reflect oxygen fugacity during the primary mineralization process. Ce_{anom} values >–0.1 reflect Ce enrichment that is indicative of an anoxic character of the sediment Ce_{anom} values <–0.1 reflect a Ce anomaly that indicates an oxic character for the sediment (Wright et al., 1987; Xie et al., 2013; Koçak, 2020). With the exception of the Eymir and Tarhana areas, samples from all other regions yielded Ce_{anom} <–0.1. In addition, regarding Eymir area, 5 samples are represented by Ce_{anom} <–0.1 and 10 samples are represented by Ce_{anom} >–0.1. For the Tarhana area, 2 samples are represented by Ce_{anom}<-0.1 and 3 samples are represented by Ce_{anom} >-0.1. In this respect, data on the Eymir and Tarhana manganese mineralization occurrences indicate that the sediment was both oxic and anoxic in character, whilst other mineralization occurrences are represented by Ce depletion (negative Ce anomaly) and an oxic water. The oxic versus anoxic character of water is related to redox conditions. In sedimentation in a reducing environment, redox conditions may change as a result of fresh water addition (e.g., via submarine currents). In many deposits, the coexistence of oxygenated and sulphur-bearing minerals is attributed to such changes.

DISCUSSION

Almost all manganese-ferromanganese mineralization associated with ophiolites comprises hydrothermal occurrences as exhalative or fault-controlled deposits that formed following the obduction of oceanic crust onto continental crust (Roy, 1992). It is inferred that mineralization in the study area had three different formation models. According to the hydrogenetic model, primary mineralization takes place by slow deposition of elements dissolved from surrounding materials under suitable Eh and pH conditions (Fig. 8A). The hydrothermal model involves either a sedimentary-exhalative type occurrence on the sea floor or a fault-controlled epigenetic stage developing on oceanic crust (Fig. 8A, B). In the hydrothermal mineralization model, seawater penetrates downwards through fractures in the oceanic crust. Changes in seawater pH are inevitable as it encounters hot oceanic crust (Roy, 1992). Modified seawater incorporates elements from the surrounding basaltic oceanic crust. Consequently, ore-forming solutions are developed which remove upwards to form hydrothermal manganese-ferromanganese deposits. The third model involves diagenesis which takes place by alteration of previously formed minerals under changing physicochemical conditions (Fig. 8B).

At low Eh and/or pH conditions, Mn is more mobile than Fe (Roy, 1992). Iron is the first element deposited, whilst manganese can stay in solution for longer. In order for iron and manganese to separate, pH must change gradually (Hem, 1972). Consequently, since iron-rich minerals are slightly immobile they are precipitated in areas close to active submarine hydrothermal centers, while manganese oxides are deposited far from these centers (Choi and Hariya, 1992). Nearly all ore samples of the AOC manganese mineralization (except for sample T1) are characterized by low Fe_2O_3 (0.04–4.44 wt.%; average 4.05 wt.%) contents. This is reflected in the scarcity of Fe-bearing minerals in the ore samples and also supported by strong negative correlation between Fe_2O_3 and MnO (r = –0.82; Appendix 1) and the absence of a positive Eu anomaly with the exception of a few samples from the Derbent (D9, D10, D11, D15, D16) and Tarhana (T1) areas. According to Sabatino et al. (2011), proximal hydrothermal Fe-Mn deposits generally display a positive Eu anomaly. Eu concentrations are gradually depleted as hydrothermal solutions travel. During ore deposition and Fe-Mn separation, Eu gradually increases. Eu anomalies are also indicative of high- (>300°C) or low-temperature (<200°C) hydrothermal alteration of oceanic crust (Michard et al., 1993). Therefore, solutions that are produced by high-temperature hydrothermal alteration are represented by a strongly positive Eu anomaly, whilst solutions that are produced by low-temperature alteration are characteristic of a weak or absent Eu anomaly (Michard et al., 1993).

Except for samples from the Cihanpasa and Buyukmahal areas, high Mn/Fe ratios (0.38–2245.10 and average 779.44) in all other samples indicate that the composition of the fluids was quite homogeneous and that the manganese deposits studied are of hydrothermal type (Nicholson, 1992a; Karakuş et al., 2010). Hydrothermal manganese deposits are also characterized by high silica contents (Jach and Dudek, 2005). The SiO_2 contents of the samples studied are 1.76–55.92 wt.% (average 17.24 wt.%; Appendix 1), indicating that the deposits were formed from hydrothermal solutions (Karakuş et al., 2010).

Trace element contents of the AOC samples are different from those of other hydrothermal deposits. In particular, there are high concentrations of Ba, Co, Cu and Sr (Appendix 1). This difference in trace element concentrations is due to diagenesis.

Separation of iron from manganese is another characteristic of diagenetic manganese deposits (Dymond et al., 1984; Jach and Dudek, 2005). Co/Zn and Co/Ni ratios have been successfully used for understanding ore-forming processes in manganese deposits (Delian, 1994; Fernandez and Moro, 1998; Öksüz, 2011a). A Co/Zn ratio of 0.15 is indicative of hydrothermal deposits and if this ratio is 2.5 or higher, Fe and Mn that form hydrogenetic deposits are accepted to be non-unique (Toth, 1980; Öksüz, 2011a).

Low trace element concentrations also indicate diagenetic processes, trace element contents of hydrogenetic Fe-Mn crusts being relatively higher (Zarasvandi et al., 2016). Trace element concentrations in the AOC (As, Ni, Pb and Zn) are lower than those of hydrogenetic deposits, but significantly higher than in hydrothermal deposits (Appendix 2 and Table 2). Mn(II) oxidation by some bacteria may increase trace element (e.g. Co) contents of manganese deposits (Moffett and Ho, 1996; Polgári et al., 2012b). Cobalt concentrations in the samples studied are relatively high in some areas (Buyukmahal 134.60–1432.10 ppm, average 621.50 ppm; Derbent 48.70–1327.80 ppm and average 367.64 ppm). As a whole, trace element concentrations in manganese ores decrease from hydrogenetic to diagenetic and hydrothermal oxide deposits (Takahashi et al., 2007; Sabatino et al., 2011). In the triangular diagram of Choi and Hariya (1992), most of the ore samples studied cluster in the hydrogenetic field although some plot in the hydrothermal field (Fig. 5C). Although this diagram shows that trace element concentrations of the ore samples studied are consistent with a hydrothermal-hydrogenetic formation, some samples have noticeably high Co contents, and tend to shift towards the hydrogenetic field (Fig. 5C). Cobalt is an important bioessential element (Moffett and Ho, 1996; Morgan, 2005) and microbially mediated reactions may increase concentrations of this element (Polgári et al., 2012b; Zarasvandi et al., 2013). The role of microbial processes in the enrichment of bioessential elements (e.g., Mn, Fe, As, Ba, Sr, Co, Ce) has been clearly shown in the Nasirabad manganese occurrence (Zarasvandi et al., 2013) and other manganese oxide deposits (Zarasvandi et al., 2016) such as non-sulphide deposits in Urkut, Hungary (Polgári et al., 2012b).

CONCLUSIONS

1. AOC manganese mineralization formed at three different stages: syngenetic, diagenetic and epigenetic.

2. A negative Eu anomaly recorded in most samples may indicate relatively little interaction with volcanic rocks during the mineralization, whilst both negative and positive anomalies observed in samples from the Derbent area might be indicative of temperature increase induced by contribution from hot hydrothermal fluids at times. The negative Eu anomaly may also show that the hydrothermal source was distant from the mineralized area or it was greatly mixed with seawater (Sabatino et al., 2011). All samples from the Cihanpasa and Buyukmahal areas are characterized by a negative Ce anomaly and simply resemble low-temperature hydrothermal mineralization. Samples from other mineralization occurrences (Derbent, Baltasarılar, Eymir and Tarhana) display both negative and positive Ce anomalies.

3. High concentrations of Ba, Co, Cu and Sr may be attributed to diagenesis. Iron separation from manganese, as typical of hydrothermal manganese occurrences, is another characteristic of diagenetic manganese deposits (Dymond et al., 1984;

Jach and Dudek, 2005). Low concentrations of trace elements such as As, Ni, Pb and Zn point to diagenetic processes (Zarasvandi et al., 2016). Trace element concentrations in the AOC mineralization are lower than those of hydrogenetic deposits, but notably higher than those of hydrothermal deposits.

4. High Ba contents, element patterns decreasing from LREE to HREE and the negative Ce anomalies imply that the ore deposits in the study area are derived from a primary hydrothermal source. However, the role of diagenetic and epigenetic processes cannot be ruled out.

REFERENCES

Adachi, M., Yamamoto, K., Sugisaki, R., 1986. Hydrothermal cherts and associated siliceous rocks from the northern Pacific: their geological significance as indication of ocean ridge activity. Sedimentary Geology, **47**: 125–148.

Akçe, M.A., Kadıoğlu, Y.K., 2005. Yozgat Batoliti kuzey bölümündeki lökogranitlerin petrolojisi (in Turkish). Geological Bulletin of Turkey, **48**: 1–20.

Bau, M., Möller, P., 1991. REE systematics as source of information on minerogenesis. In: Source, Transport and Deposition of Metals (eds. M. Pagel and J.L. Leroy): 17–20. Balkema, Rotterdam.

Bellanca, A., Masetti, D., Neri, R., 1997. Rare earth elements in limestone/marlstone couplets from the Albian-Cenomanian Cismon section (Venetian region, northern Italy): assessing REE sensitivity to environmental changes. Chemical Geology, **141**:141–152.

Bonatti, E., Kraemer, T., Rydell, H., 1972. Classification and genesis of submarine iron-manganese deposits. In: Ferromanganese Deposits on the Ocean Floor: International Decade on Ocean Exploration (ed. D. Horn): 149–166. National Science Foundation, Washington, D.C.

Boztuğ, D., Harlavan, Y., Arehart, G.B., Satır, M., Avcı, N., 2007. K/Ar age, whole-rock and isotope geochemistry of A-type granitoids in the Divrigi-Sivas region, eastern-central Anatolia, Turkey. Lithos, **97**: 193–218.

Choi, J.H., Hariya, Y., 1992. Geochemistry and depositional environment of Mn oxide deposits in the Tokoro Belt, Northeastern Hokkaido, Japan. Economic Geology, **87**: 1265–1274.

Crerar, D.A., Namson, J., Chyi, M.S., Williams, L., Feigenson, I.M., 1982. Manganiferous cherts of the Fransiscan assemblage: I. General geology, ancient and modern analogues, and implications for hydrothermal convection at oceanic spreading centers. Economic Geology, **77**: 519–540.

De Carlo, E.H., Mc Murtry, G.M., 1992. Rare earth element geochemistry of ferromanganese crusts from the Hawaiian Archipelago, central Pacific. Chemical Geology, **95**: 235–250.

De Baar, H.J.W., German, C.R., Elderfield, H., Van Gaans, P., 1988. Rare earth element distributions in anoxic waters of the Cariaco Trench. Geochimica et Cosmochimica Acta, **52**: 1203–1219.

Del Rio Salas, R., Ruiz, J., Ochoa-Landin, L., Noriega, O., Bara, F., Meza-Figueroa, D., Paz-Moreno, F., 2008. Geology, geochemistry and Re-Os systematics of manganese deposits from the Santa Rosalia Basin and adjacent areas in Baja California Sur, Mexico. Mineralium Deposita, **43**: 467–482.

Delian, F., 1994. Geological and Geochemical Research of the Manganese Ore Bed (in Chinese), M1. Weather Publishing Press, Beijing.

Dymond, J., Lile, M., Finnely, B., Piper, D.Z., Murphy, K., Conard, R., Pisias, N., 1984. Ferromanganese nodules from MANOP sites H, S, and R: control of mineralogical and chemical compo-

sition by multiple accretionary processes. Geochimica et Cosmochimica Acta, **48**: 931–949.

Evensen, M.N., Hamilton, P., O'Nions, R.K., 1978. Rare earth abundances in chondritic meteorites. Geochimica et Cosmochimica Acta, **42**: 1199–1212.

Fernandez, A., Moro, M.C., 1998. Origin and depositional environment of Ordovician stratiform iron mineralization from Zamora (NW Iberian Peninsula). Mineralium Deposita, **33**: 606–619.

Fitzgerald, C.E., Gillis, K.M., 2006. Hydrothermal manganese oxide deposits from Baby Bare seamount in the Northeast Pacific Ocean. Marine Geology, **225**: 145–156.

Fleet, H.J., Henderson, P., Kepme, D.D.C., 1976. Rare earth element and related chemistry of some drilled Southern Indian Ocean basalts and volcanogenic sediments. Journal of Geophysical Research, **81**: 4257–4268.

German, C.R., Elderfield, H., 1989. Rare earth elements in Saanich Inlet, British Columbia, a seasonally anoxic basin. Geochimica et Cosmochimica Acta, **53**: 2561–2571.

Glasby, G.P., Stüben, D., Jeschke, G., Stoffers, P., Garbe-Schönberg, C.D., 1997. A model for the formation of hydrothermal manganese crusts from the Pitcairn Island hotspot. Geochimica et Cosmochimica Acta, **61**: 4583–4597.

Hein, J.R., Schulz, M.S., Kang, J.K., 1990. Insular and submarine ferromanganese mineralization of the Tonga-Lau region. Marine Mining, **9**: 305–354.

Hein, J.R., Schulz, M.S., Gein, L.M., 1992. Central Pacific cobalt rich ferromanganese crusts. Historical perspective and regional variability. Circum Pacific Council for Energy and Mineral Resources. Earth Science Series, **14**: 261–283.

Hein, J.R., Kochinsky, A., Halbach, P., Manheim, F.T., Bau, M., Kang, J.K., Lubick, N., 1997. Iron and manganese oxide mineralization in the Pacific. Geological Society Special Publications, **119**: 123–138.

Hein, J.R., Schulz, M.S., Dunham, R.E., Stern, R.J., Bloomer, S.H., 2008. Diffuse flow hydrothermal manganese mineralization along the active Mariana and southern Izu-Bonin arc system, western Pacific. Journal of Geophysical Research, **113**: B08S14.

Hem, J.D., 1972. Chemical factors that influence that influence the availability of iron and manganese in aqueous systems. GSA Bulletin, **83**: 443–450.

Heshmatbehzadi, K., Shahabpour, J., 2010. Metallogeny of manganese and ferromanganese ores in Baft Ophiolitic Mélange, Kerman, Iran. Australian Journal of Basic and Applied Sciences, **4**: 302–313.

Hodkinson, R.A., Stoffers, P., Scholten, P., Cronan, D.S., Jeschke, G., Rogers, T.D.S., 1994. Geochemistry of hydrothermal manganese deposits from the Pitcairn Island hotspot, Southeastern Pacific. Geochimica et Cosmochimica Acta, **58**: 5011–5029.

Jach, R., Dudek, T., 2005. Origin of a Toarcian manganese carbonate/silicate deposit from the Krízna unit, Tatra Mountains, Poland. Chemical Geology, **224**: 136–152.

Kadıoğlu, Y., Dilek, Y., Foland, K.A., 2006. Slab break-off and syncollisional origin of the Late Cretaceous magmatism in the Central Anatolian crystalline complex, Turkey. GSA Bulletin, **409**: 381–415.

Karakuş, A., Yavuz, B., Koç, S., 2010. Mineralogy and major- trace element geochemistry of the Haymana manganese mineralizations, Ankara, Turkey. Geochemistry International, **48**: 1014–1027.

Kato, Y., Yamaguchi, K.E., Ohmoto, H., 2006. Rare earth elements in Precambrian banded iron formations: secular change of Ce and Eu anomalies and evolution of atmospheric oxygen. GSA Bulletin, **198**: 269–289.

Kato, Y., Fujinaga, K., Nakamura, K., Takaya, Y., Kitamura, K., Ohta, J., Toda, R., Nakashima, T., Iwamori, H., 2011. Deep-sea mud in the Pacific Ocean as a potential resource for rare earth elements. Nature Geoscience, **4**: 535–539.

Ketin, I., 1966. Tectonic units of Anatolia. Bulletin of the Mineral Research and Exploration Institute, Turkey, **66**: 20–34.

Koç, S., Özmen, O., Öksüz, N., 2000. Geochemical characteristics defining the formation environment of Kasimaga (Keskin-Kirikkale) manganese oxide mineralization (in Turkish). Bulletin of the Mineral Research and Exploration Institute, Turkey, **122**: 107–118.

Koçak, I., 2020. Sarıhıdır manganese mineralization related to travertine, Central Anatolian Volcanic Province, Turkey. Geodinamica Acta, **32**: 11–24.

Köksal, S., Romer, R.L., Göncüoğlu, M.C., Toksoy-Köksal, F., 2004. Timing of post-collisional H-type to A-type granitic magmatism: U-Pb titanite ages from Alpine central Anatolian granitoids (Turkey). International Journal of Earth Sciences, **93**: 974–989.

Kunzendorf, H., Glasby, G.P., 1994. Minor and rare earth elements in manganese crusts and nodules and sediments from the Manihiki Plateau and adjacent areas: results of HMNZS Tui Cruises. Marine Georesources and Geotechnology, **12**: 271–281.

Maynard, J.B., 2010. The chemistry of manganese ores through time: a signal of increasing diversity of earth-surface environments. Economic Geology, **105**: 535–552.

Michard, A., Michard, G., Stuben, D., Stoffers, P., Cheminee, J.L., Binard, N., 1993. Submarine thermal springs associated with young volcanoes: the Teahitia vents, Society Islands Pacific Ocean. Geochimica et Cosmochimica Acta, **57**: 4977–4986.

Michard, A., 1989. Rare earth element systematics in hydrothermal fluids. Geochimica et Cosmochimica Acta, **53**: 745–750.

Mills, R.A., Wells, D., Roberts, S., 2001. Genesis of ferromanganese crusts from the TAG hydrothermal field. Chemical Geology, **176**: 3–293.

Moffett, J.W., Ho, J., 1996. Oxidation of cobalt and manganese in seawater via a common microbially catalyzed pathway. Geochimica et Cosmochimica Acta, **60**: 3415–3424.

Monnin, C., Wheat, C.G., Dupre, B., Elderfield, H., Mottl, M.J., 2001. Barium geochemistry in sediment pore waters and formation waters of the oceanic crust on the eastern flank of the Juan de Fuca Ridge (ODP Leg 168). Geochemistry, Geophysics, Geosystems, **2**: 1008.

Morgan, J.J., 2005. Kinetics of reaction between O_2 and Mn(II) species in aqueous solutions. Geochimica et Cosmochimica Acta, **69**: 35–48.

Nath, B.N., Balaram, V., Sudhakar, M., Plüger, W.L., 1992. Rare earth element geochemistry of ferromanganese deposits of the Indian Ocean. Marine Chemistry, **38**: 185–208.

Nayan, J., Rongfen, J., Ziyu, W., 1994. Permian Palaeogeography and Geochemical Environment in Lower Yangtze Region, China. Petroleum Industry Press, Beijing.

Nicholson, K., 1992a. Contrasting mineralogical-geochemical signatures of manganese oxides: guides to metallogenesis. Economic Geology, **87**: 1253–1264.

Nicholson, K., 1992b. Genetic types of manganese oxide deposits in Scotland: indicators of paleoocean-spreading rate and a Devonian geochemical mobility boundary. Economic Geology, **87**: 1301–1309.

Okay, A., 2008. Geology of Turkey: a synopsis. Anschnitt, **21**: 19–42.

Okay, A.I., Tüysüz, O., 1999. Tethyan sutures of northern Turkey. Geological Society Special Publications, **156**: 475–515.

Öksüz, N., 2011a. Geochemistry and the origin of manganese mineralizations in Derbent (Yozgat) Region (in Turkish). Bulletin for Earth Sciences, Hacettepe University, Turkey, **32**: 213–234.

Öksüz, N., 2011b. Geochemical characteristics of the Eymir (Sorgun-Yozgat) manganese deposit, Turkey. Journal of Rare Earths, **29**: 287–296.

Öksüz, N., Okuyucu, N., 2014. Mineralogy, geochemistry, and origin of Buyukmahal manganese mineralization in the Artova Ophiolitic Complex, Yozgat, Turkey. Journal of Chemistry, 2014, http://dx.doi.org/10.1155/2014/837972

Özcan, A., Erkan, E., Keskin, A., Oral, A., Ozer, S., Sumengen, M., Tekeli, O., 1980. North Anatolian fault and Kırşehir massive search for the basic geology. Bulletin of the Mineral Research and Exploration, Turkey, **6722**.

Öztürk, H., 1993. Turkish manganese deposits. Jounal of Geo-Engineering, **43**: 24–33.

Peters, T., 1988. Geochemistry of manganese-bearing cherts associated with Alpine-ophiolites and the Hawasina formations in Oman. Marine Geology, **84**: 229–238.

Polgári, M., Hein, J.R., Toth, A., Pal-Molnar, E., Vigh, T., Bíró, L., Fintor, K., 2012a. Microbial action formed Jurassic Mn-carbonate ore deposit in only a few hundred years (Urkut, Hungary). Journal of Geology, **40**: 903–906.

Polgári, M., Hein, J.R., Vigh, T., Szabó-Drubina, M., Fórizs, I., Bíró, L., Müller, A., Tóth, A.L., 2012b. Microbial processes and the origin of the Úrkút manganese deposit, Hungary. Ore Geology Reviews, **47**: 87–109.

Polgári, M., Németh, T., Pál-Molnár, E., Futo, I., Vigh, T., Mojzsis, S.J., 2016. Correlated chemostratigraphy of Mn-carbonate microbialites (Úrkút, Hungary). Gondwana Research, **29**: 278–289.

Robertson, A.H.F., Fleet, A.J., 1976. The origins of rare earths in metalliferous sediments of the Troodos Massif, Cyprus. Earth and Planetary Science Letters, **28**: 385–394.

Roy, S., 1992. Environments and processes of manganese deposition. Economic Geology, **87**: 1218–1236.

Ruhlin, D.E., Owen, R.M., 1986. The rare earth element geochemistry of hydrothermal sediments from the East Pacific Rice: examination of a seawater scavenging mechanism. Geochimica et Cosmochimica Acta, **50**: 393–400.

Sabatino, N., Neri, R., Bellanca, A., Jenkyns, H.C., Masetti, D., Scopelliti, G., 2011. Petrography and high-resolution geochemical records of Lower Jurassic manganese-rich deposits from Monte Mangart, Julian Alps. Palaeogeography, Palaeoclimatology, Palaeoecology, **299**: 97–109.

Shah, M.T., Moon, C.J., 2007. Manganese and ferromanganese ores from different tectonic settings in the NW Himalayas, Pakistan. Journal of Asian Earth Sciences, **29**: 455–465.

Sugisaki, R., 1984. Relation between chemical composition and sedimentation rate of Pacific Ocean floor sediments deposited since the middle Cretaceous: basic evidence for chemical constraints on depsitional environments of ancient sediments. Journal of Geology, **92**: 235–259.

Şasmaz, A., Yavuz, F., Sağıroğlu, A., Akgül, B., 2005. Geochemical patterns of the Akdagmadeni (Yozgat, Central Turkey) fluorite deposits and implications. Journal of Asian Earth Sciences, **24**: 469–479.

Şasmaz, A., Turkyilmaz, B., Öztürk, N., Yavuz, F., Kumral, M., 2014. Geology and geochemistry of Middle Eocene Maden complex ferromanganese deposits from Elazig-Malatya region, Eastern, Turkey. Ore Geology Reviews, **56**: 352–372.

Şengör, A.M.C., Yilmaz, Y., 1981. Tethyan evolution of Turkey: a plate tectonic approach: Tectonophysics, **75**: 181–241.

Takahashi, Y., Manceau, A., Geoffroy, N., Marcus, M.A., Usui, A., 2007. Chemical and structural control of the partitioning of Co, Ce and Pb in marine ferromanganese oxides. Geochimica et Cosmochimica Acta, 71: 984–1008.

Taylor, S.R., McLennan, S.M., 1985. The Continental Crust, Its Composition and Evolution. Blackwell, Oxford.

Temiz, H., Ozden, S., Guezou, J.C., 2010. Izmir-Ankara-Erzincan Kenet Kusagi'nin Artova-Camlibel (Tokat) kesiminin Gec Neojen'deki tektonik deformasyon bicimi ve kinematigi (in Turkish). Cumhuriyet Science Journal, 27: 71–89.

Toth, J.R., 1980. Deposition of submarine crusts rich in manganese and iron. GSA Bulletin, 91: 44–54.

Tüysüz, O., Dellaloğlu, A.A., 1992. Geologic evolution of Cankiri Basin and its tectonic units. 9th Petroleum Congress of Turkey Uctea Chamber of Geophysical Engineers Turkish Association of Petroleum Geologists Uctea Chamber of Petroleum Engineers, Hilton Ankara: 333–349.

Usui, A., Mita, N., 1995. Geochemistry and mineralogy of a modern buserite deposit from a hot spring in Hokkaido, Japan. Clays and Clay Minerals, 43: 116–127.

Usui, A., Someya, M., 1997. Distribution and composition of marine hydrogenetic and hydrothermal manganese deposits in the northwest Pacific. Journal of the Geological Society, 119: 177–198.

Whitney, D.L., Teyssier, C., Fayon, A.K., Hamilton, M.A., Heizler, M., 2003. Tectonic controls on metamorphism, partial melting, and intrusion: timing and duration of regional metamorphism and magmatism in the Nigde Massif, Turkey. Tectonophysics, 376: 37–60.

Wright, J., Schrader, H., Holser, W.T., 1987. Paleoredox variations in ancient oceans recorded by rare earth elements in fossil apatite. Geochimica et Cosmochimica Acta, 51: 631–644.

Xie, J.C., Yang, X.Y., Du, J.G., Xu, W., 2006. Geochemical characteristics of sedimentary manganese deposit of Guichi, Anhui Province, China. Journal of Rare Earths, 24: 374–380.

Yalınız, M.K., Floyd, P.A., Göncüoğlu, M.C., 1996. Supra-subduction zone ophiolites of Central Anatolia: geochemical evidence from the Sarğkaraman Ophiolite, Aksaray, Turkey. Mineralogical Magazine, 60: 697–710.

Zarasvandi, A., Pourkaseb, H., Sepahvand, M.R., Raith, J., Rezaei, M., 2016. Tracing of hydrothermal ore forming process in the Sorkhvand manganese deposit, Kermanshah Province, Iran. Arabian Journal of Geoscience, 9: 109.

Zarasvandi, A., Lentz, D., Rezai, M., Pourkaseb, H., 2013. Genesis of the Nasirabad manganese occurrence, Fars province, Iran: geochemical evidences. Chemie der Erde, 73: 495–508.